Journal of Alloys and Compounds 511 (2012) 85–89

Contents lists available at SciVerse ScienceDirect

Journal of Alloys and Compounds

journal homepage: www.elsevier.com/locate/jallcom

Thermoelectric properties of p-type Pb-doped $Bi_{85}Sb_{15-x}Pb_x$ alloys at cryogenic temperatures

Z. Chen[a,b], M. Zhou[a], R.J. Huang[a], C.M. Song[c], Y. Zhou[a], L.F. Li[a,*]

[a] Key Laboratory of Cryogenics, Technical Institute of Physics and Chemistry, Chinese Academy of Sciences, Beijing 100190, PR China
[b] Graduate University of Chinese Academy of Sciences, Beijing 100049, PR China
[c] Department of Physics, Zunyi Normal College, Zunyi 563002, PR China

ARTICLE INFO

Article history:
Received 4 February 2011
Received in revised form 20 August 2011
Accepted 22 August 2011
Available online 26 August 2011

Keywords:
Thermoelectric materials
Mechanical alloying
Electrical transport
Thermal conductivity

ABSTRACT

In this study we have investigated the effect of the Pb on the thermoelectric propertied of Bi–Sb alloy with different Pb-content. The Pb-doped $Bi_{85}Sb_{15-x}Pb_x$ ($x = 0$, 0.5, 1, 2, 3) alloys were synthesized by mechanical alloying followed by pressureless sintering. The crystal structure was characterized by X-ray diffraction. The Seebeck coefficients, electrical conductivities, and thermal conductivities were measured in the temperature range of 77–300 K. The results show that all the Pb-doped alloys are p-type thermoelectric materials in the whole measurement temperature range. A minimum thermal conductivity of 1.7 W/mK was obtained for $Bi_{85}Sb_{12}Pb_3$ sample at 150 K. A maximum ZT value of 0.11, which is higher than those previous reported, was obtained for $Bi_{85}Sb_{14}Pb_1$ at 210 K.

1. Introduction

Thermoelectric materials have attracted considerable attention during past decades due to their usage both as generators which directly convert thermal energy into electricity and as refrigeration devices which directly pump heat from a cold side to a hot side. In contrast to traditional mechanical refrigeration or a generator, thermoelectric devices take advantage of no moving parts, quiet operation, low environmental impact and high reliability. The performance of a thermoelectric material is described by a dimensionless thermoelectric figure of merit, ZT, which is calculated using the relation $ZT = \alpha^2\sigma T/\kappa$, where α, σ, κ, and T are, respectively the Seebeck coefficient (thermoelectric power), electrical conductivity, thermal conductivity and absolute temperature [1]. Accordingly, thermoelectric materials with high-performance can be expected through a combination of a relatively high Seebeck coefficient, high electrical conductivity and low thermal conductivity.

During the past years, the performance of conventional thermoelectric materials and new high-performance thermoelectric materials, such as Bi–Te alloys [2,3], Pb–Te alloys [4–7], oxides [8–10] and half-Heusler compounds [11,12], low-dimensional thermoelectric materials [13,14], has been improved. However, the progress of thermoelectric materials which are applied below room temperature was relatively limited [15,16]. In fact, low-temperature thermoelectric materials have wide potential applications in cooling of precision devices, such as laser diodes, charge-coupled device cameras, infrared detectors. At low temperature, it is reported that monocrystalline Bi–Sb alloys exhibit the best thermoelectric performance [17,18]. Their results indicated that the Z values of $Bi_{88}Sb_{12}$ single crystals and $Bi_{85}Sb_{15}$ single crystals could reach to $5.5 \times 10^{-3}\,K^{-1}$ [17] and $6.5 \times 10^{-3}\,K^{-1}$ at around 80 K [18], respectively. By the application of a magnetic field, the thermoelectric performance of $Bi_{85}Sb_{15}$ alloy is found to be improved, and in such a case the Z value could reach to $11 \times 10^{-3}\,K^{-1}$ at 100 K [18]. However, it is very difficult to produce good homogenous single crystals of $Bi_{100-x}Sb_x$, and the poor mechanical properties of these single crystals limit the manufacturing. Distinct from single crystal materials, poly-crystalline materials may be more suitable for applications for thermoelectric devices [19]. Moreover, previous results have shown that the thermoelectric properties of poly-crystalline Bi–Sb alloys can be improved by doping effect [20–22]. For example, it was reported that Bi–Sb alloys with Z value of $1.79 \times 10^{-3}\,K^{-1}$ at 196 K was obtained through partial substitution of Nb for Sb [23]. Bulk $Bi_{100-x}Sb_x$ exhibits an n-type semiconductor behavior when $7 < x < 22$ or a semimetal character when $x \leq 7$ and $x \geq 22$ [24,25]. At present, for cooling below room temperature, Bi–Sb alloys have been used in the n-type legs, coupled with p-type legs of $(Bi,Sb)_2(Te,Se)_3$ [26,27]. In 2004, it was found that the ZT value of the p-type single crystal $CsBi_4Te_6$ reached to 0.82 at 225 K by doping with SbI_3 [28]. This result suggests that $CsBi_4Te_6$ may be useful

* Corresponding author. Tel.: +86 10 8254 3698; fax: +86 10 8254 3700.
E-mail address: laifengli@mail.ipc.ac.cn (L.F. Li).

0925-8388/$ – see front matter © 2011 Elsevier B.V. All rights reserved.
doi:10.1016/j.jallcom.2011.08.076

for developing low-temperature thermoelectric devices. However, the temperature range of the optimum *ZT* of this p-type material is higher than that of n-type Bi–Sb alloys, so that they may not be a good match in a thermoelectric element. On the other hand, the thermal conductivities as well as the coefficients of thermal expansion of these two materials are both different, which may cause serious problems for practical application. Therefore, an identical matrix material that could be prepared both as n-type and as p-type is always desired. P-type Bi–Sb based alloys have been obtained by doping Pb or Sn at Sb site [17,18,22,29]. A large power factor of 1.2×10^{-3} W/mK^2 at 220 K has been demonstrated for a 3 at.% Sn-doped $Bi_{88}Sb_{12}$ sample, with a large positive Seebeck coefficient [22]. Nevertheless, the *ZT* value is still not large enough to satisfy the practical requirement. Therefore it is significant to improve the thermoelectric performance of p-type Bi–Sb based thermoelectric materials.

In the present study, a series of p-type $Bi_{85}Sb_{15-x}Pb_x$ (x = 0.5, 1, 2, 3) thermoelectric materials were prepared by mechanical alloying and subsequent pressureless sintering processes. The phase composition of the novel p-type alloys was investigated by X-ray diffraction. The effects of Pb-doping on the thermoelectric and transport properties are interpreted.

2. Experimental details

The $Bi_{85}Sb_{15-x}Pb_x$ (x = 0, 0.5, 1, 2, 3) alloys were prepared by mechanical alloying in a planetary ball mill with stainless steel jars and balls. The ball-to-powder weight ratio was 20:1 and the rotation speed was fixed at 350 rpm. Powders of Bi (nominal purity 5 N), Sb (nominal purity 6 N) and Pb (nominal purity 3 N) all with initial particle size of about 100 μm were put into a vessel, and then the vessel was hermetically sealed under argon to prevent oxidation. After 50 h milling, the milled powders were pressed into pellets under 1 GPa and then the obtained circular sample was heat treated at 473 K in a tube furnace under argon for 2 h.

X-ray diffraction (XRD) with a Rigaku D/max-RB diffractometer (Cu Kα radiation λ = 0.154 nm) was employed to reveal the phase compositions. The temperature dependence of electrical conductivity, Seebeck coefficient and thermal conductivity were measured in the temperature range of 77–300 K. The electrical conductivity was characterized by using a four-probe method. The Seebeck coefficient was determined from measured temperature and electric potential difference between the two ends of the bar-shaped specimen. The thermal conductivity was measured by means of a steady-state method. To investigate the thermoelectric behavior, Hall coefficient (R_H), carrier concentration (n) and Hall mobility (μ_H) were determined using a PPMS (physical property measurement system) under a constant magnetic field of 9.0 T.

3. Results and discussion

3.1. Structure characterization

Fig. 1 shows the X-ray diffraction (XRD) patterns of the $Bi_{85}Sb_{15-x}Pb_x$ (x = 0, 0.5, 1, 2, 3). It is found that the Pb-doped $Bi_{85}Sb_{15-x}Pb_x$ (x = 0.5, 1, 2, 3) alloy has a dominating phase with Bi–Sb structure (the space group $R\bar{3}m$). No other visible diffraction peaks in the samples of the low Pb doping contents (x < 2) are observed, which indicates that Pb enters completely into the Bi–Sb lattice and substitutes of Sb during the synthesis process. However, small peaks of the Pb_7Bi_3 phases (PDF#39-1087, JCPDS-ICDD, JCPDS-International Center for Diffraction Data, 12 Campus Bouleavard, Newtown Square, PA, USA, 2004) are detected in the patterns of $Bi_{85}Sb_{15-x}Pb_x$ (x = 2, 3) alloys, as shown in Fig. 1. Moreover, it is found that the relative intensities of these diffraction peaks increase with the increase of Pb element. These results indicate that the excess Pb doping helps Pb_7Bi_3 phases appear in the $Bi_{85}Sb_{15-x}Pb_x$ alloys.

The lattice parameters evaluated from the X-ray diffraction patterns is shown in Table 1. It is found that the parameters gradually increase with the Pb doping. This result is well consistent with the fact that the radius of Sb atom is smaller than that of Pb atom, and indirectly reveals that Sb atoms were successfully substituted by Pb.

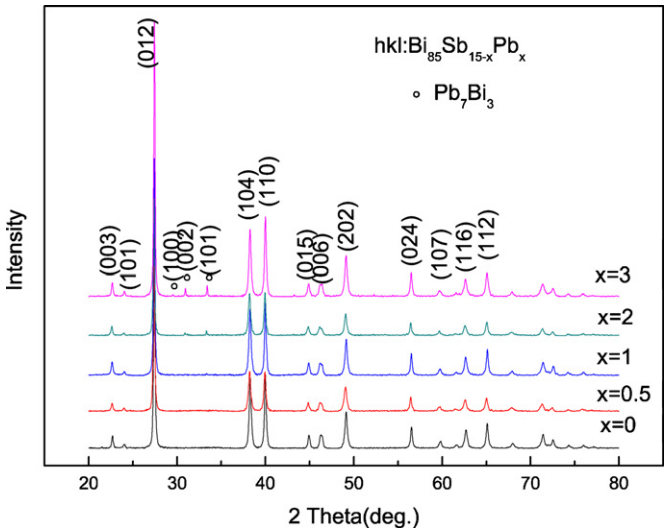

Fig. 1. X-ray diffraction patterns for the $Bi_{85}Sb_{15-x}Pb_x$ (x = 0, 0.5, 1, 2, 3) samples.

Table 1
The lattice parameters and the crystalline sizes of the $Bi_{85}Sb_{15-x}Pb_x$ (x = 0, 0.5, 1, 2, 3) samples.

	x = 0	x = 0.5	x = 1	x = 2	x = 3
a (nm)	0.45054	0.45101	0.45071	0.45099	0.45034
c (nm)	1.17727	1.17834	1.17894	1.18064	1.17693

3.2. Electrical conductivity and Seebeck coefficient

Fig. 2 shows the temperature dependence of the electrical conductivity of $Bi_{85}Sb_{15-x}Pb_x$ (x = 0, 0.5, 1, 2, 3) in the temperature range of 77–300 K. It is observed that the electrical conductivity increases with temperature for the un-doped $Bi_{85}Sb_{15}$ alloy, indicating a typical semiconducting behavior. However, it is found that the electrical conductivities decrease with temperature for all the doped alloys, indicating a semimetal behavior. This is because

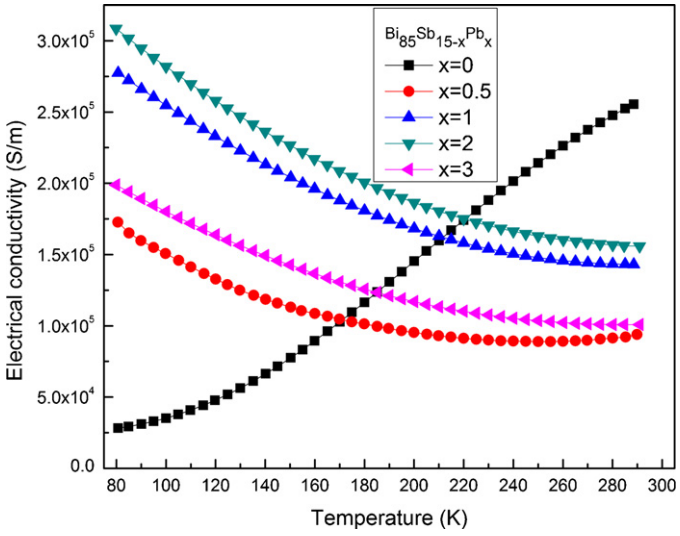

Fig. 2. The electrical conductivities as a function of temperature for the $Bi_{85}Sb_{15-x}Pb_x$ (x = 0, 0.5, 1, 2, 3) samples.

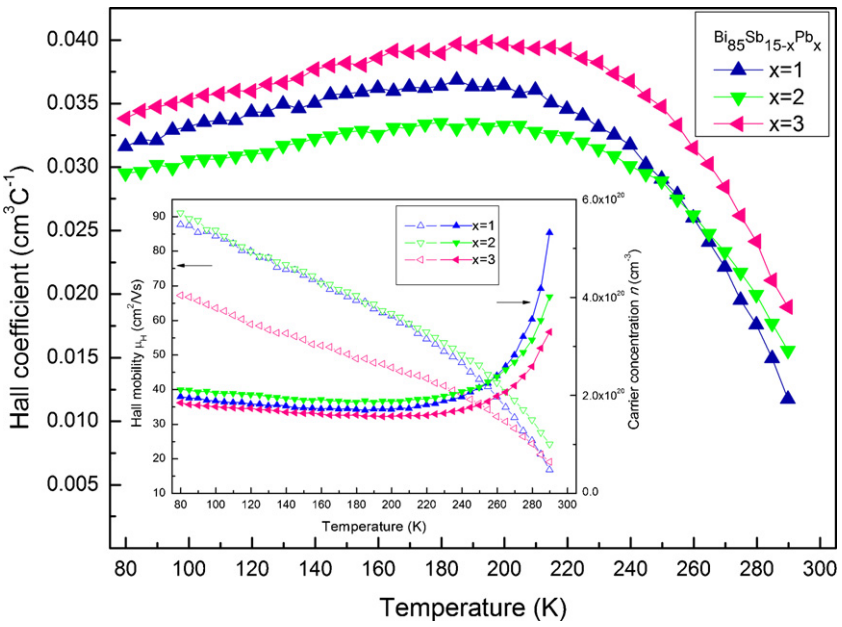

Fig. 3. Temperature-dependent Hall coefficient, carrier concentration and Hall mobility (lower left corner) of the $Bi_{85}Sb_{15-x}Pb_x$ ($x = 1, 2, 3$) samples.

the Group IV element Pb acts as an acceptor in the semiconducting Bi–Sb alloys and lowers the Fermi level, effectively resulting in a one-carrier dominant material. Therefore the electrical conductivity of the doped alloy is found to increase with decreasing temperature, which may be due to the enhanced concentration of the holes around substituted Sb site.

The electrical conductivities of the Pb-doped alloys are found to increase with small x. However, reverse behavior is observed when x is larger than 2. It is found that the $Bi_{85}Sb_{15-x}Pb_x$ ($x = 2$) alloy exhibits the highest electrical conductivity and a maximum value of 3.1×10^5 S/m is observed at 77 K. The electrical conductivity of an isotropic material under zero magnetic field can be assessed by $\sigma = ne\mu + pe\nu$, where n and p are the densities of electrons and holes and μ and ν are their mobilities, respectively. Carrier mobility is inversely proportional to the scattering factor, which includes grain boundary scattering, defect scattering, charge carrier scattering and so on. Although the concentration of carriers could be increased by increasing the molar fraction of Pb, the disorder effect and the structure defects induced by the Pb doping lead to a decrease in carrier mobility. In addition, the formation of Pb_7Bi_3 in the alloys disorder the lattice structures of the Bi–Sb based alloys, resulting in the decreasing of mobility. Consequently, the balance of the two competing factors, charge carrier concentration (n or p) and mobility (μ or ν), determines the overall electrical conductivity.

To estimate the concentration and Hall mobility of the carriers, Hall effect measurements were performed. The carrier concentration was calculated from the experimentally measured Hall coefficient, R_H, assuming a single carrier model and a Hall scattering factor of unity, by $n = 1/(R_H e)$, where e is the electron charge. The Hall mobility, μ_H, was calculated from $\mu_H = R_H\sigma$. Typical results of the carrier concentration and mobility as functions of testing temperature of the samples are plotted in Fig. 3. The carrier concentration is found to increase firstly and then to decrease when x is larger than 2. At high temperature, the concentration increases rapidly which results from the intrinsic excitation of carriers. Moreover, the calculated Hall mobility agrees with the above speculation that σ could possibly change.

Fig. 4 shows the Seebeck coefficient as a function of temperature for the $Bi_{85}Sb_{15-x}Pb_x$ ($x = 0$, 0.5, 1, 2, 3) alloys. It is found that the Seebeck coefficient is positive for all the doped alloys, indicating a p-type electrical transport behavior. Moreover, it is observed that it does not change sign at elevated temperatures, which is different from the former report [22]. This result is in line with the result of Hall coefficient measurement. The Seebeck coefficient of these alloys is found to increase monotonically up to 200 K and then to decrease at elevated temperature. The maximum value of the Seebeck coefficient is obtained for the $Bi_{85}Sb_{14.5}Pb_{0.5}$ alloy, which is 101 μV/K at around 210 K. The relationship between the Seebeck coefficient and the carrier concentration (n) can be expressed as $\alpha = \gamma - \ln n$, where γ is a scattering rate, which results from grain

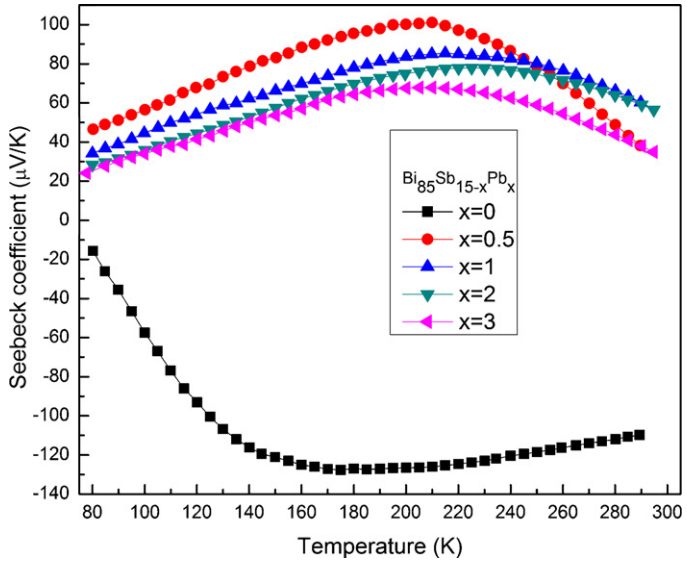

Fig. 4. The Seebeck coefficients as a function of temperature for the $Bi_{85}Sb_{15-x}Pb_x$ ($x = 0$, 0.5, 1, 2, 3) samples.

Table 2
Estimation of the Fermi energy E_F of the $Bi_{85}Sb_{15-x}Pb_x$ ($x = 0$, 0.5, 1, 2, 3) samples.

	$x = 0$	$x = 0.5$	$x = 1$	$x = 2$	$x = 3$
E_F (eV)	0.12	−0.15[a]	−0.18[a]	−0.20[a]	−0.23[a]

[a] The minus sign signifies that the Fermi energy is below the valence band edge.

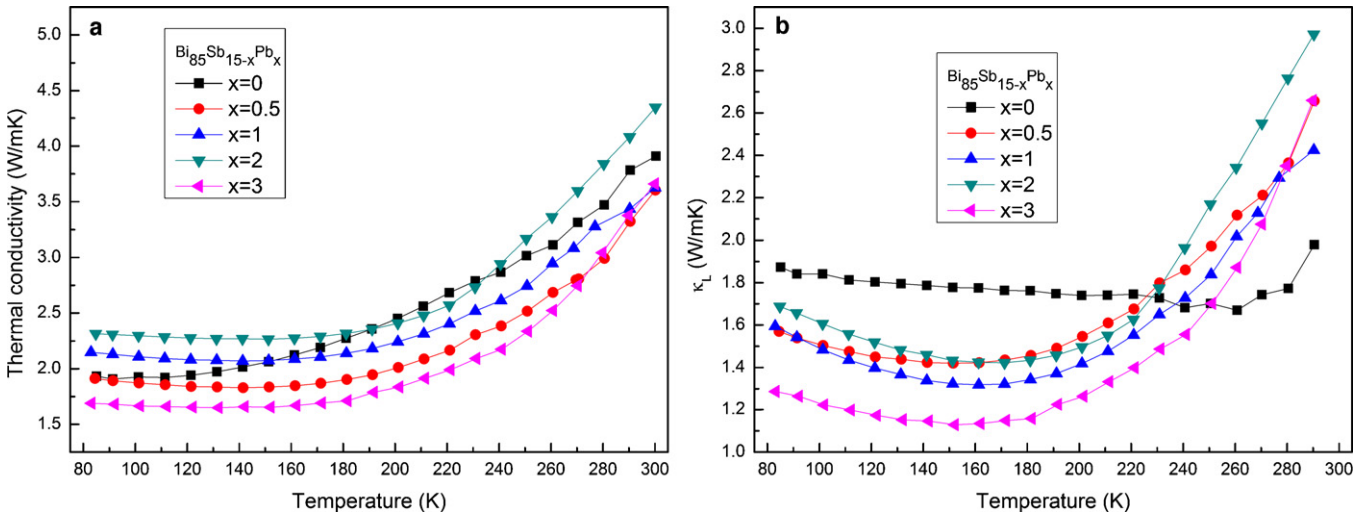

Fig. 5. The total thermal conductivities (a) and the lattice contribution κ_L of the thermal conductivities (b) as a function of temperature for the $Bi_{85}Sb_{15-x}Pb_x$ ($x = 0, 0.5, 1, 2, 3$) samples, respectively.

boundary scattering and charge carrier scattering. Therefore, the increase of the Seebeck coefficients may be caused by the dominant effect of carrier scatterings in point defects and grain boundaries resulting from the introduction of Pb. The reason for the decrease of the Seebeck coefficients may be because the rapid increase of carrier concentration n with the rise in temperature, and the ambipolar contribution arising from the diffusion of electron–hole pairs with the onset of intrinsic contribution.

The Seebeck coefficient, which is the most sensitive among the electron transport properties, can provide valuable information on the electronic structure near the Fermi energy surface [30]. The general expression for the diffusion Seebeck coefficient in the degenerate free-electron approximation is given by the Mott's relation [30]:

$$\alpha = -\frac{\pi^2 {k_B}^2 T}{3e}\left[\frac{d\ln\sigma(E)}{dE}\right]_{E=E_F},$$

where k_B is the Boltzmann's constant, e is elementary charge, and E_F is the Fermi energy. For a pure metal, the diffusion thermoelectric power is $\alpha = \pi^2 {k_B}^2 T/(eE_F)$ at temperatures where electron–phonon scattering is dominant [25,31]. Even though the above expression for thermoelectric power holds good for metals, we can approximately calculate the Fermi energy using this equation for degenerate regime of the doped Bi–Sb alloys since they are degenerate narrow band gap semiconductors. Like the previous report, the Fermi energy is found to decrease with increasing Pb concentration [25]. The derived Fermi energies of these alloys at 210 K are shown in Table 2.

3.3. Thermal conductivity

Fig. 5 shows the thermal conductivities and the lattice thermal conductivities as a function of temperature. The thermal conductivities of all the alloys are found to increase with temperature and the minimum thermal conductivity is about 1.7 W/mK for $Bi_{85}Sb_{12}Pb_3$ at 150 K. The thermal conductivity κ is mainly the sum of the lattice contribution κ_L and the electronic contribution κ_e associated with the free carriers. The electronic contribution to κ_e was calculated using the Wiedemann–Franz law assuming the Lorenz number to be 2.45×10^{-8} W Ω/K^2 (for degenerate semiconductors). And the lattice thermal conductivities were obtained

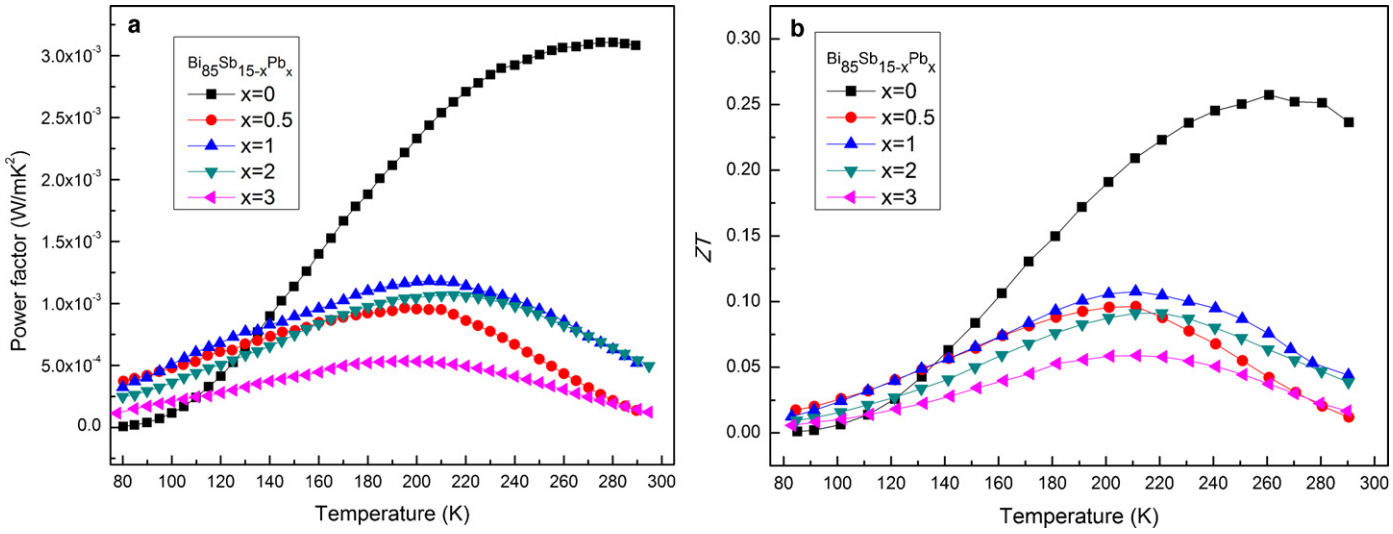

Fig. 6. The power factor (a) and the figure-of-merit (b) as a function of temperature for the $Bi_{85}Sb_{15-x}Pb_x$ ($x = 0, 0.5, 1, 2, 3$) samples, respectively.

by subtracting the electrical contribution from the total thermal conductivity using the equation $\kappa_L = \kappa - \kappa_e$ (as shown in Fig. 5(b)). Lattice contribution κ_L is proportional to the phonon mean free path, which is mainly determined by the lattice vibration and is relevant to the microstructure. As shown in Fig. 5, the lattice thermal conductivity κ_L of all the Pb doped alloys is found to decrease with temperature below 160 K, and then to increase with temperature. The decrease of κ_L below 160 K stems mainly from the enhanced electron–phonon scattering. Lattice thermal conductivity is observed to increase rapidly at elevated temperature, as shown in Fig. 5(b). This is because the ambipolar contribution arising from the diffusion of electron–hole pairs with the onset of intrinsic contribution, which is consistent with results in Ref. [32]. The lattice thermal conductivity of Pb doped $Bi_{85}Sb_{15-x}Pb_x$ samples is lower than that of the un-doped $Bi_{85}Sb_{15}$ sample, which can be attributed to the mass-fluctuation scattering between dopant Pb (atomic mass $M_{Pb} \approx 207$) and Sb (atomic mass $M_{Sb} \approx 122$). Moreover, it is found that lattice thermal conductivity of $Bi_{85}Sb_{12}Pb_3$ is lower than those of all the other samples, which results from the scattering by structural defects that caused by the Pb_7Bi_3 impurity.

3.4. Power factor and figure-of-merit

The temperature dependence of power factors and *ZT* values is plotted in Fig. 6(a) and (b), respectively. It is observed that the power factor increases with temperature and then drops when temperature is higher than 200 K. The power factors of all Pb-doped $Bi_{85}Sb_{15-x}Pb_x$ alloys are found to be lower than that of the un-doped $Bi_{85}Sb_{15}$. This can be ascribed to the degradation of electrical transport properties, especially the decrease in the absolute value of the Seebeck coefficient. A maximum power factor of 1.18×10^{-3} W/mK^2 was obtained for $Bi_{85}Sb_{14}Pb_1$ at 205 K. This value is very close to that of the $(Bi_{88}Sb_{12})_{97}Sn_3$ alloy prepared by direct melting, quenching, and annealing treatment [22]. As shown in Fig. 6(b), it is observed that the behavior of the *ZT* values is similar to those of the power factors. Moreover, a largest *ZT* value of 0.11 is achieved for $Bi_{85}Sb_{14}Pb_1$ at 210 K. This value is significantly larger than that of $Bi_{0.885}Sb_{0.075}Sn_{0.04}$ (0.08 at 200 K) due to the relatively higher Seebeck coefficients [29].

4. Conclusions

$Bi_{85}Sb_{15-x}Pb_x$ ($x = 0$, 0.5, 1, 2, 3) alloys have been fabricated through mechanical alloying and subsequently pressureless sintering method. X-ray diffraction analysis confirms that all the alloys crystallize with a rhombohedral crystal structure. With appropriate substitution of Pb for Sb, the electrical transport properties of the Bi–Sb alloys change from n-type to p-type. Among all the Pb-doped p-type alloys, the $Bi_{85}Sb_{14}Pb_1$ shows a largest *ZT* value of 0.11 at 210 K. Consequently, Pb-doped $Bi_{85}Sb_{15-x}Pb_x$ alloys are expected to be promising p-type thermoelectric materials used at low temperature.

Acknowledgment

This project is supported by National Natural Science Foundation of China (No. 51066008 and No. 50802101).

References

[1] F. DiSalvo, Science 285 (1999) 703–706.
[2] B. Poudel, Q. Hao, Y. Ma, Y.C. Lan, A. Minnich, B. Yu, X. Yan, D.Z. Wang, A. Muto, D. Vashaee, X.Y. Chen, J.M. Liu, M.S. Dresselhaus, G. Chen, Z. Ren, Science 320 (2008) 634–638.
[3] X. Fan, J. Yang, W. Zhu, S. Bao, X. Duan, Q. Zhang, J. Alloys Compd. 448 (2008) 308–312.
[4] K.F. Hsu, S. Loo, F. Guo, W. Chen, J.S. Dyck, C. Uher, T. Hogan, E.K. Polychroniadis, M.G. Kanatzidis, Science 303 (2004) 818–821.
[5] M. Zhou, J.F. Li, T. Kita, J. Am. Chem. Soc. 130 (2008) 4527–4532.
[6] P. Zhu, Y. Imai, Y. Isoda, Y. Shinohara, X. Jia, G. Zou, J. Alloys Compd. 420 (2006) 233–236.
[7] B. Paul, P. Banerji, J. Appl. Phys. 109 (2011) 103710.
[8] C. Ruttanapun, A. Wichainchai, W. Prachamon, A. Yangthaisong, A. Charoenphakdee, T. Seetawan, J. Alloys Compd. 509 (2011) 4588–4594.
[9] R. Robert, L. Bocher, B. Sipos, M. Döbeli, A. Weidenkaff, Prog. Solid State Chem. 35 (2007) 447–455.
[10] N.V. Nong, C.J. Liu, M. Ohtaki, J. Alloys Compd. 509 (2011) 977–981.
[11] P.J. Lee, L.S. Chao, J. Alloys Compd. 504 (2010) 192–196.
[12] M. Schwall, B. Balke, Appl. Phys. Lett. 98 (2011) 042106.
[13] T. Harman, P. Taylor, M. Walsh, B. LaForge, Science 297 (2002) 2229–2232.
[14] T. Harman, M. Walsh, B. laforge, G. Turner, J. Electron. Mater. 34 (2005) 19–22.
[15] L. Pan, X.Y. Qin, H.X. Xin, D. Li, J.H. Sun, J. Zhang, C.J. Song, R.R. Sun, Intermetallics 18 (2010) 1106–1110.
[16] J.E. Rodríguez, L.C. Moreno, Mater. Lett. 65 (2011) 46–48.
[17] G.E. Smith, R. Wolfe, J. Appl. Phys. 33 (1962) 841–846.
[18] W.M. Yim, A. Amith, Solid-State Electron. 15 (1972), 1141–1144, IN1143–IN1144, 1145–1165.
[19] K. Hiroyuki, N. Hiroyuki, T. Kiyabu, I. Masaki, N. Yasutoshi, J. Phys. Chem. Solids 65 (2004) 1223–1227.
[20] C.B. Thomas, H.J. Goldsmid, J. Phys. D: Appl. Phys. 3 (1970) 333–336.
[21] B. Lenoir, M. Cassart, M. Kinany-Alaoui, H. Scherrer, S. Scherrer, The Thirteenth International Conference on Thermoelectrics, AIP, 1994, pp. 230–234.
[22] H. Noguchi, H. Kitagawa, T. Kiyabu, K. Hasezaki, Y. Noda, J. Phys. Chem. Solids 68 (2007) 91–95.
[23] C. Song, R. Huang, M. Zhou, L. Gong, L. Li, J. Phys. Chem. Solids 71 (2010) 999–1003.
[24] B. Lenoir, M. Cassart, J. Michenaud, H. Scherrer, S. Scherrer, J. Phys. Chem. Solids 57 (1996) 89–99.
[25] S. Cho, A. Divenere, G.K. Wong, J.B. Ketterson, J.R. Meyer, J. Appl. Phys. 85 (1999) 3655–3660.
[26] G. Snyder, E. Toberer, Nat. Mater. 7 (2008) 105–114.
[27] N.A. Sidorenko, L.D. Ivanova, Inorg. Mater. 37 (2001) 331–335.
[28] D.Y. Chung, T.P. Hogan, M. Rocci-Lane, P. Brazis, J.R. Ireland, C.R. Kannewurf, M. Bastea, C. Uher, M.G. Kanatzidis, J. Am. Chem. Soc. 126 (2004) 6414–6428.
[29] Y. Hor, R. Cava, J. Alloys Compd. 479 (2009) 368–371.
[30] R. Barnard, Thermoelectricity in Metals and Alloys, Taylor and Francis, London, 1972.
[31] S. Dutta, V. Shubha, T.G. Ramesh, F. D'Sa, J. Alloys Compd. 467 (2009) 305–309.
[32] J.L. Cui, H.F. Xue, W.J. Xiu, L.D. Mao, P.Z. Ying, L. Jiang, J. Alloys Compd. 460 (2008) 426–431.